Pairing and superconductivity in the flat band: Creutz lattice

Rubem Mondaini,[1] G. G. Batrouni,[2,3,4,1] and B. Grémaud[3,4,5,6,7]
[1]*Beijing Computational Science Research Center, Beijing 100193, China*
[2]*Université Côte d'Azur, INPHYNI, CNRS, 0600 Nice, France*
[3]*MajuLab, CNRS-UCA-SU-NUS-NTU International Joint Research Unit, 117542 Singapore*
[4]*Centre for Quantum Technologies, National University of Singapore, 2 Science Drive 3, 117542 Singapore*
[5]*Department of Physics, National University of Singapore, 2 Science Drive 3, 117542 Singapore*
[6]*Laboratoire Kastler Brossel, UPMC-Sorbonne Universités, CNRS, ENS-PSL Research University, Collége de France, 4 Place Jussieu, 75005 Paris, France*
[7]*Aix Marseille Université, Université de Toulon, CNRS, CPT, Marseille, France*

(Received 28 June 2018; revised manuscript received 5 September 2018; published 25 October 2018)

We use unbiased numerical methods to study the onset of pair superfluidity in a system that displays flat bands in the noninteracting regime. This is achieved by using a known example of flat band systems, namely, the Creutz lattice, where we investigate the role of local attractive interactions in the $U < 0$ Hubbard model. Going beyond the standard approach used in these systems where weak interactions are considered, we map the superfluid behavior for a wide range of interaction strengths and exhibit a crossover between BCS and tightly bound bosonic fermion pairs. We further contrast these results with a standard two-leg fermionic ladder, showing that the pair correlations, although displaying algebraic decay in both cases, are longer ranged in the Creutz lattice, signifying the robustness of pairing in this system.

DOI: 10.1103/PhysRevB.98.155142

I. INTRODUCTION

Systems exhibiting flat (dispersionless) bands come in many varieties and manifest a wide range of interesting phenomena such as exotic superfluid phases, edge states, topological insulator/superconductor phases, and bound Majorana fermion edge states to name a few. For example, at half-filling in the Lieb lattice (which belongs to a large family of flat band models) [1–7], the fermionic Hubbard model with repulsive contact interaction U has a ground state with nonzero spin [8], while in the absence of Hubbard interaction, a particle in the flat band is geometrically localized on four sites due to quantum interference in the hopping terms [9]. On the other hand, the attractive Hubbard model on the same lattice exhibits unusual charge and charge transfer signatures within the flat band and reduced pairing order when either the flat band starts to be occupied or when it is completely filled [10]. It has also been argued that fermionic pairing in flat bands would lead to more robust pairs and higher critical temperatures [11]. Remarkable experiments have recently shown [12] that graphene bilayers twisted by about 1.1° exhibit an ultraflat band at the charge neutrality point. This leads to a correlated insulator which, when doped, becomes superfluid.

Another very interesting class of systems has the lowest band flat, e.g., sawtooth [13], kagome, Creutz [14], and many others [15]. In the ground state of such systems, there is a critical density below which each particle is geometrically localized over a few sites (which depends on the lattice geometry) and such that the localized particles do not interact. Exceeding the critical density causes the particle wave functions to overlap and interaction ensues, thus destroying localization. Such systems have been recently studied extensively both in fermionic and bosonic models. In the latter case, it was shown in a fully frustrated chain (diamond lattice, which has three flat bands when threaded by a π flux) that when interactions are included in such a way to reduce the original local U(1) symmetry to a discrete local Z_2 gauge symmetry, a new exotic phase appears, namely a nematic superfluid where the current is supported by bosons paired on different sites[16], or using a fermionic language by the condensation of pairs of Cooper pairs [17]; the same system was later studied for spinless fermions [18]. In the sawtooth lattice, it was found that doping above the critical density leads to a phase where the peak of the momentum distribution is at nonzero momentum [13], while doping the kagome lattice leads to a supersolid phase [13]. Adding longer-range interactions between the bosons on the sawtooth lattice uncovers topological effects such as the Haldane insulator phase and edge states in open systems [19]. Bosons were also studied on the flat band Creutz lattice (Fig. 1) leading to a rich phase diagram exhibiting a condensate, a pair condensate, a supersolid and phase separation phases [20,21].

Fermions in such systems, where the flat band is the lowest, are very interesting for a variety of reasons. They have been shown to exhibit a plethora of topological effects such as edge states [14], which are robust to interactions when in the presence of induced pairing terms [22]. A general treatment of fermions with attractive interactions in nontrivial flat bands, where the Chern number $\mathcal{C} \neq 0$, demonstrated [23] that such systems are guaranteed to exhibit nonzero superfluid weight $D_s \geqslant |\mathcal{C}|$. In the case of quasi-one-dimensional systems, in particular, the Creutz lattice, with $\mathcal{C} = 0$, it was shown [24] that the superfluid weight is $D_s \geqslant |\mathcal{W}|^2$, where $\mathcal{W}$ is the winding number.

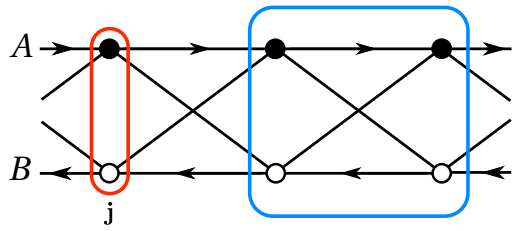

FIG. 1. The Creutz lattice [14]. The (red) rectangle encloses a unit cell, the (blue) square shows the geometry of the localized states in the absence of interactions when the particle density is less than the critical value 1/2. The arrows depict the sign of the hopping in the intrachain bonds. In the interchain bonds, the hopping energies have the same magnitude.

Here, we study numerically the Creutz model with an attractive Hubbard interaction, $U < 0$, using the density matrix renormalization group (DMRG) and exact diagonalization (ED). We calculate the superfluid weight, the Drude weight D_s in one dimension, for various fillings as a function of $|U|$ and show that for small $|U|$ the predictions of Ref. [24] are accurate, i.e., the superfluid weight grows linearly with the strength of the interactions for densities away from half-filling. Going beyond the small $|U|$ regime, the model is shown to map onto a hardcore bosonic model for large enough $|U|$. As a measure of the robustness of superfluidity, we calculate the one- and two-particle gaps, and the decay exponents of the pair correlation functions for the Creutz flat band model and compare with the normal two-leg model. We find that pair correlations decay algebraically with distance, whereas single-particle ones decay exponentially, for finite values of the interactions. Furthermore, we find that for all the parameters we studied, the power-law decay is slower, often much slower, in the Creutz lattice than in the normal two-leg model.

II. MODEL

We study the attractive Hubbard model on the Creutz lattice [14] (see Fig. 1), governed by the Hamiltonian

$$\begin{aligned}\mathcal{H} = &-it\sum_{j,\sigma}\left(c^{A\dagger}_{j,\sigma}c^{A}_{j+1,\sigma} - c^{B\dagger}_{j,\sigma}c^{B}_{j+1,\sigma} + \text{H.c.}\right)\\ &-t\sum_{j,\sigma}\left(c^{A\dagger}_{j,\sigma}c^{B}_{j+1,\sigma} + c^{B\dagger}_{j,\sigma}c^{A}_{j+1,\sigma} + \text{H.c.}\right)\\ &+U\sum_{j,\alpha} n^{\alpha}_{j,\uparrow}n^{\alpha}_{j,\downarrow},\end{aligned} \tag{1}$$

where the onsite interaction, U, is negative; A and B label the two chains, t connects both inter- and intrachain sites j and $j+1$ and the sum over j spans L unit cells. The fermion spin is labeled by $\sigma = \uparrow, \downarrow$ and $\alpha = A, B$ is the chain index. This Hamiltonian governs a balanced population of up and down spins making inter- and intrachain hops and interacting attractively when on the same site.

It is worth noting that applying a local gauge transformation, $c^{A}_{j,\sigma} \to \exp(-i\pi j/2)c^{A}_{j,\sigma}$ and $c^{B}_{j,\sigma} \to \exp(-i\pi(j-1)/2)c^{B}_{j,\sigma}$, renders all the hopping terms real. The intrachain hopping parameter on chain A (B) becomes t ($-t$); interchain hopping between site j on chain A (B) and site $j+1$ on chain B (A) is given by $-t$ (t). When applied to a lattice with periodic boundary conditions, the number of unit cells must be a multiple of four for this transformation to apply, whereas for the case of open boundary conditions, it works for any system size. This proved to be very useful in some of our DMRG calculations on large lattices, as one has to deal with a purely real Hamiltonian. One must note that, in general, local gauge transformations do not change the topological class of the system as long as the relevant symmetries are consistently modified when changing gauge [25].

For $U = 0$, $\mathcal{H}$ can be diagonalized [14,20,21] revealing two flat bands, $E_{\pm} = \pm 2t$. Consequently, when a particle is placed in the lattice, it will be localized on four sites, shown by the blue square in Fig. 1. The localized ground states are given by

$$\left|\Psi^{\text{loc}}_{j,\sigma}\right\rangle = -\tfrac{1}{2}[c^{B\dagger}_{j,\sigma} + ic^{B\dagger}_{j+1,\sigma} + ic^{A\dagger}_{j,\sigma} + c^{A\dagger}_{j+1,\sigma}]|0\rangle. \tag{2}$$

For $U \geqslant 0$, i.e., repulsive interactions, all states are thus localized as long as the filling is less than half, $\rho \equiv (N_{\uparrow} + N_{\downarrow})/N_s \leqslant 1/2$, where N_{σ} is the total number of fermions with spin σ and $N_s = 2L$ is the number of sites. The ground-state energy is then trivially given by $E(\rho \leqslant 1/2) = -2tN_s\rho$, and the chemical potential is constant, $\mu = -2t$ resulting in infinite compressibility. When $U < 0$, the fermions can lower their energy further by pairing and, consequently, they are no longer geometrically localized. This is the situation we shall study here. We note that this model is different from that treated in Ref. [22], where the spin of the fermion changes when it performs interchain hops but it does not change for intrachain hops.

Our system is like that considered in Ref. [24], where hopping does not induce spin change, and where it is shown that the Bardeen-Cooper-Schrieffer (BCS) wave function is an exact eigenstate of an effective Hamiltonian, valid at low energies. In this regime, one obtains that the system is infinitely compressible and the eventual coupling to the upper band results in a finite compressibility, accompanied by an algebraic decay of the pair Green function.

III. METHODOLOGY AND RESULTS

We employed complementary approaches to study pairing in this attractive model at different filling fractions. If the attractive interaction induces up and down fermions to form pairs, the resulting composite bosons (not necessarily local) may delocalize, yielding a superfluid/superconducting phase. Such behavior would be signaled by power-law decay of the pair correlation function, $G^{\alpha\beta}_{p}(r)$, and exponential decay of the single-particle Green function, $G^{\alpha\beta}_{\sigma}(r)$ [26,27],

$$G^{\alpha\beta}_{p}(r) = \left\langle \Delta^{\alpha\dagger}_{j+r}\Delta^{\beta}_{j}\right\rangle, \tag{3}$$

$$G^{\alpha\beta}_{\sigma}(r) = \left\langle c^{\alpha\dagger}_{j+r,\sigma}c^{\beta}_{j,\sigma}\right\rangle, \tag{4}$$

$$\Delta^{\alpha}_{j} \equiv c^{\alpha}_{j,\uparrow}c^{\alpha}_{j,\downarrow}, \tag{5}$$

where Δ^{α}_{j} is a pair annihilation operator at site j on chain α, and $\alpha = A, B$ and $\beta = A, B$ label the chains. We mostly focus on the case where $\alpha = \beta$, i.e., intrachain correlators. As

detailed below, we study these correlation functions by means of DMRG [28,29] on large lattices (up to $L = 192$) with open boundary conditions. The remaining quantities are obtained with periodic boundary conditions, as we describe below.

Another important physical quantity characterizing transport is the superfluid weight D_s given, in one dimension by [30–35]

$$D_s = \pi L \frac{\partial^2 E_0(\Phi)}{\partial \Phi^2}\bigg|_{\Phi=0}. \tag{6}$$

Here, $E_0(\Phi)$ is the ground-state energy in the presence of a phase twist Φ applied via the replacement $c_j^\alpha \to e^{i\phi j} c_j^\alpha$, where $\phi = \Phi/L$ is the phase gradient. This endows the hopping terms with a phase $\exp(i\phi)$ (or its complex conjugate).[1]

As explained in Ref. [34], taking the thermodynamic limit, $L \to \infty$, and computing the curvature are noncommuting operations in two and three dimensions. The Drude weight, D, is obtained by computing the curvature for finite lattices, and extrapolating it to the thermodynamic limit. On the other hand, the superfluid weight, D_s, is obtained by computing first the ground-state energy $E_0(L, \Phi)$ for lattice size L, extrapolating to the thermodynaimc limit and then calculating the curvature. However, in one dimension [34], the two operations do commute: the curvature of the ground state is essentially related to the Drude weight. One, therefore, needs further diagnostics to identify the superfluid phase. For bosonic systems, world line algorithms allow direct computation of the superfluid density [36]. However, for the Creutz lattice, the localization of the states due to the flat bands leads to a vanishing Drude weight for the noninteracting system and therefore the superfluid weight, D_s, and the Drude weight, D, are essentially equivalent and given by Eq. (6). For the regular two-leg ladder, we will see below that this is not so. Even for $|U| \to 0$, the right-hand side of Eq. (6) does not vanish and actually corresponds to the noninteracting Drude weight. However, this does not mean that the system is superfluid at $|U| = 0$. To determine if the system is superconducting, we examine the single-particle and the pairing Green functions. We identify a superconducting phase by the exponential decay of the former and power-law decay of the latter. With this caveat in mind, we use the notation D_s to which we refer equivalently as the Drude or superfluid weight.

A. Superfluid weight: Creutz lattice

We focused on four different fillings: $\rho_f = 1$, 3/4, 1/2, and 1/4, using a combination of exact diagonalization (ED) for smaller lattice sizes and DMRG for the larger ones, with periodic boundary conditions (PBC) in both cases. In the former, we were restricted to lattices that are commensurate with those fillings, and such that the reduced Hilbert space sizes, at different momentum sectors of the translation-invariant Eq. (1), are $\lesssim 10^8$. For example, in the fillings $\rho_f = 1/2$ and 1/4, the largest system sizes tackled using ED had $L = 10$ and 16, respectively. Nonetheless, the DMRG results complemented these for larger lattices, where we have kept up to 1200 states in the truncation process and checked that the results were unchanged when more states are kept. It is well known that imposing PBC strongly degrades the efficiency of DMRG. One of the reasons is that PBC results in an effective long-range coupling between the first and last sites. On the other hand, as displayed in Fig. 2, one can fold the system with PBC to a ladderlike structure with OBC and vanishing couplings between the two legs of the ladder for all sites but the first and last two ones. Of course, this amounts to doubling the size of the local Hilbert space, i.e., for each rung, which, in turn, would require a larger bond dimension. Still, we have checked that for usual 1D chains (bosons or fermions), the DMRG convergence is much better than with the standard way of implementing PBC.

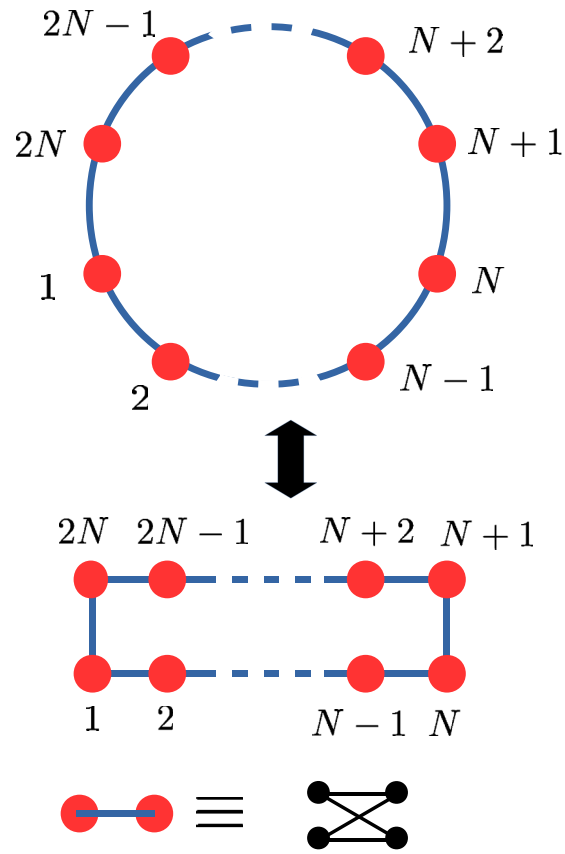

FIG. 2. Mapping a system with periodic boundary condition to a ladderlike structure. The ring shape structure of the system with PBC is folded to ladderlike structure with OBC and vanishing couplings between the two legs of the ladder for all sites but the first and the last.

We start by reporting on Figs. 3(a)–3(c), the ground-state energy E_0 in Eq. (1) with $|U|/t = 8$, as a function of Φ_f [hereafter, $\Phi = \Phi_f$, for the fermionic Hamiltonian (1)], for different system sizes and fillings. When we subtract the zero gauge contribution, $E_0(\Phi_f) = 0$, and rescale by the system size, we notice that, at half filling, the curvature decreases

[1]We emphasize that if using open boundary conditions, a local gauge transformation can be applied to remove the phases ϕ in the hopping terms. Likewise, in the case of periodic boundary conditions, a similar transformation relates the two equivalent cases: when the phase Φ is spread over the bonds and when they are accumulated at the boundaries, such that only one bond has a twist $c_L^\alpha \to e^{i\Phi} c_1^\alpha$.

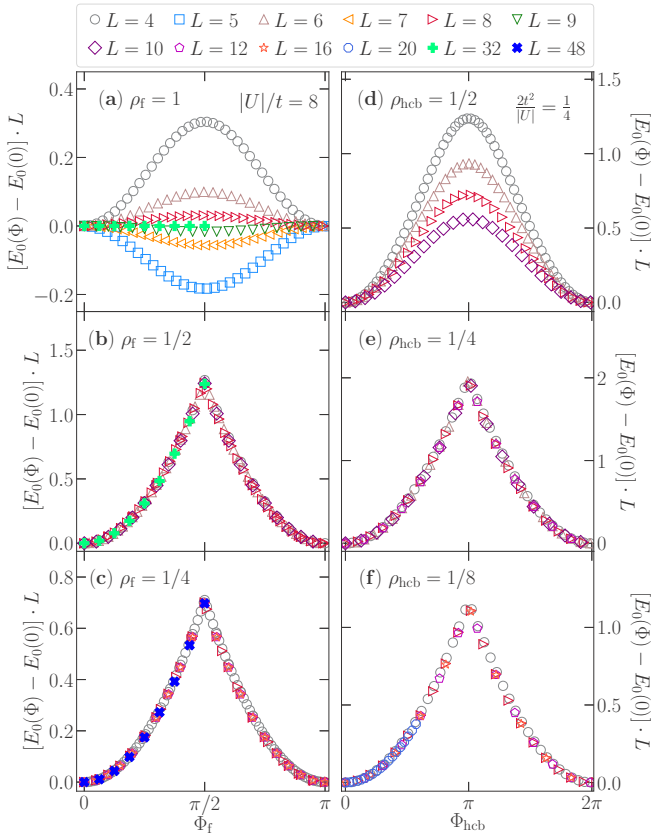

FIG. 3. Dependence of the ground-state energy on the applied flux Φ that threads the lattice, for the fermionic Hamiltonian (1) [(a)–(c)], and for the effective hard-core boson Hamiltonian (8) [(d)–(f)]. In the former, we use $|U|/t = 8$ and in the latter, $J = V = 2t^2/8$. The densities in (a)[(d)], (b)[(e)], and (c)[(f)] are $\rho_f = 1$ ($\rho_{hcb} = 1/2$), $\rho_f = 1/2$ ($\rho_{hcb} = 1/4$), and $\rho_f = 1/4$ ($\rho_{hcb} = 1/8$). The filled (empty) symbols depict the DMRG (ED) results.

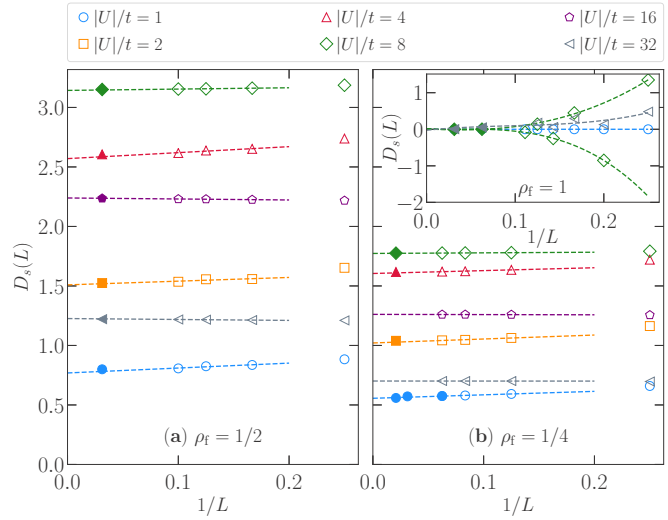

FIG. 4. Extrapolation of D_s to the thermodynamic limit for three different fermionic densities: (a) $\rho_f = 1/2$, (b) $1/4$, and (inset) 1, with different values of interactions U. The open (full) symbols were obtained with ED (DMRG); lines in the main panels are linear fits for the larger systems sizes. In the inset, we use an exponential fit and notice a typical even and odd effect related to the formation of closed shells, also seen in other contexts as, for example, in the Drude weight for the 1d Hubbard model [33]. It is seen that the two methods yield consistent results and give finite extrapolations for D_s when $L \to \infty$, for densities other than $\rho_f = 1$.

as the system size increases. This is in stark contrast with the cases with densities $\rho_f < 1$ [Figs. 3(b) and 3(c)], where they are rather insensitive to L. This is the first indication that superfluidity is manifest only away from half-filling.

Finite size scaling of the curvatures is displayed in Fig. 4, to probe the results when approaching the thermodynamic limit; it shows clearly that $D_s(L \to \infty)$ is finite for $U < 0$ and $\rho_f < 1$. At half-filling [inset in Fig. 4(b)], the system displays a vanishing superfluid weight, for a large range of interactions. Moreover, D_s has a nonmonotonic dependence on U away from half-filling. It grows as the strength of the attractive interactions grows until $|U|/t \approx 8$, where it starts to decrease in the strongly interacting regime.

Finally, by compiling the values of D_s extrapolated to the thermodynamic limit, we construct in Fig. 5 the dependence of the superfluidity on the interactions for different densities, where the nonmonotonic behavior is evident. Essentially, the interactions induce a crossover betwen two regimes, at small and large values of $|U|/t$. As mentioned in Introduction, and explained in detail in Ref. [23], the superfluid weight (Drude weight in 1D) for a multiband system, computed within a mean-field BCS approach, is the sum of three different terms. One of the terms is the usual single-band BCS term and vanishes for a flat band, whereas the other two terms have a topological origin, i.e., related to the fact that the band structure has a nontrivial Berry curvature in two dimensions or a nonzero winding number in one. In the present situation, neglecting the contribution from the upper band, i.e., in the limit $U \ll t$, one has [24]

$$D_s = \pi |U| \rho (1 - \rho). \tag{7}$$

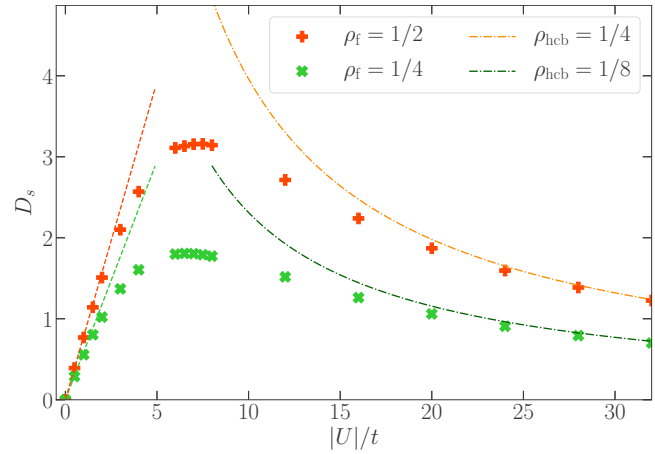

FIG. 5. D_s, for $L \to \infty$, vs $|U|/t$, highlighting the nonmonotonic behavior of the superfluidity. For small interactions, D_s increases linearly with slope $\pi\rho(1-\rho)$ (see text). At large $|U|/t$, the decay can be explained by an effective Hamiltonian of repulsive hardcore bosons in a Creutz geometry, Eq. (8). These are represented by the dashed-dotted lines.

This linear dependence on $|U|/t$ is plotted in Fig. 5 for $\rho = 1/2,\ 1/4$, as dashed lines, and is seen to be in excellent agreement with our exact numerical values for small $|U|/t$.

On the other hand, at large $|U|/t$, the $\uparrow$ and $\downarrow$ fermions form strongly bound pairs being approximately described by a *local* bosonic particle. Given the constraints on the occupancy for each site, one can show that in this case, the fermionic Hamiltonian (1) can then be mapped onto a Hamiltonian of *repulsive* hardcore bosons whose hopping and near-neighbor repulsion have the same energy scale [37], and the density of particles is $\rho_{\rm hcb} = \rho_{\rm f}/2$. The effective Hamiltonian then reads

$$\mathcal{H}_{\rm eff} = -\frac{2t^2}{|U|}\sum_{j,\alpha,\beta}\left(b_j^{\alpha\dagger}b_{j+1}^{\beta} + \text{H.c.}\right) + \frac{2t^2}{|U|}\sum_{j,\alpha,\beta}\left(n_j^{\alpha}n_{j+1}^{\beta} + n_{j+1}^{\beta}n_j^{\alpha}\right), \tag{8}$$

where $n_j^{\alpha} = b_j^{\alpha\dagger}b_j^{\alpha}$, and $b_j^{\alpha\dagger}$ (b_j^{α}) is a hardcore boson creation (annihilation) operator on site j and chain $\alpha = A,\ B$. They satisfy $\{b_j^{\alpha}, b_j^{\alpha\dagger}\} = 1$, and $[b_j^{\alpha}, b_r^{\beta\dagger}] = 0$ for $j \neq r$ or $\alpha \neq \beta$. We note that this effective model is defined on the Creutz lattice, Fig. 1, but is not governed by a Creutz Hamiltonian as in Eq. (1), i.e., the hopping bonds are preserved but in this case they all have the *same* hopping energy. Thus the Hamiltonian (8) is not flat: it describes hardcore bosons on a quasi-one-dimensional lattice with a nonflat dispersion relation and which are expected to be superfluid.

Analogously to what we have done with the fermionic Hamiltonian, we numerically studied the effect of a phase gradient on the hopping terms, implemented via the replacement $b_j^{\alpha} \to e^{i\phi j}b_j^{\alpha}$ [$\phi/L \equiv \Phi_{\rm hcb}$], in order to probe the superfluid properties of this effective model. The dependence of the ground-state energy on the flux $\Phi_{\rm hcb}$ is shown in Figs. 3(d)–3(f), using ED for different system sizes. First, we notice the curvatures display a similar qualitative behavior. At half-filling, the curvature of $E_0(\Phi)\cdot L$ decreases for increasing system sizes while it is independent of L for densities away from it. Second, the periodicity of the $E_0(\Phi)$ curve in the bosonic case is twice as large as in the fermionic one. This is an expected result based on considerations of flux quantization of superconducting rings [38,39]. A magnetic flux enclosed by such a ring is related to a vector potential manifested along the direction of the lattice as $\vec{A} = (\varphi/L)\hat{x}$. This, in turn, results in a twist of the boundary conditions along the same direction of the form $\exp\{i2\pi\varphi/\varphi_0\}$, where φ_0 is the flux quantum hc/e. Byers and Yang [38] have shown that the energies are periodic functions of φ, whose period is φ_0/n, where n is the total charge of the basic group. For instance, for superconductors with carriers of charge $2e$, $n = 2$. In our units, the period Φ of the ground-state energy in the fermionic problem is π, which correcting the 2π factor, results in periods $\varphi = \varphi_0/2$, i.e., Cooper pairing superconductivity, as expected. On the other hand, for the case of effective hardcore boson model, the period of the ground-state energy with Φ is 2π, that results in periods $\varphi = \varphi_0/1$, i.e., the charge of the superfluid carrier is one, a hardcore boson itself.

Beyond the qualitative description of the mapping between the two models, we show that the agreement is also quantitative for large interactions. Computing the superfluid weight via Eq. (6) and extrapolating to the thermodynamic limit (not shown), we obtain D_s for the hardcore boson effective model [Eq. (8)], which we display as dashed-dotted lines in Fig. 5. For large values of $|U|/t$, the *fermionic* superfluid weight asymptotically approaches the one for hardcore bosons, further confirming the local nature of the pairs in this regime and its superfluid character for densities away from half-filling.

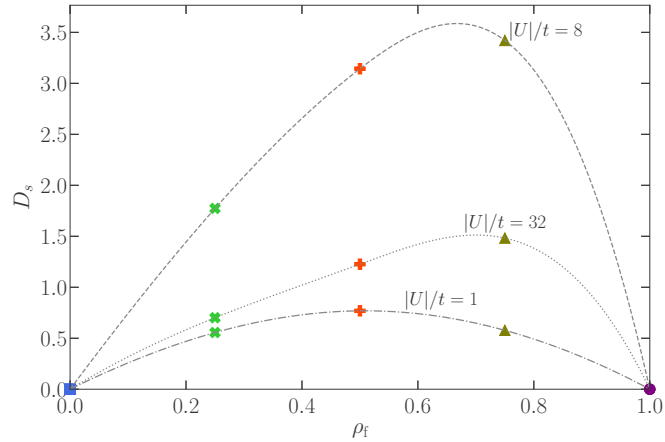

FIG. 6. Dependence of the superfluid weight on the total fermionic density, for different interaction strengths: With small interactions ($|U|/t = 1$), where the description of the projected Hamiltonian is suitable, at large interactions ($|U|/t = 32$) and around the peak of D_s for the intermediate fillings ($|U|/t = 8$).

Turning back to the fermionic problem, Fig. 6 displays the dependence of the superfluid weight on the total density $\rho_{\rm f}$ for different interaction strengths. In the noninteracting case, due to the dispersionless nature of the bands, the superfluid weight is zero regardless of the density investigated. When the interactions are finite but small, such that the ground state can still be described by a BCS wave function, the superfluid weight follows a form predicted by Eq. (7), symmetric in the densities around $\rho_{\rm f} = 1/2$. Away from this regime, increasing the interactions, causes D_s to become asymmetric, with its peak moving to higher filling.

B. Excitation gaps

We further characterize the transport properties of the system by studying the nature of particle excitations. In particular, we study the fate of one- and two-particle excitations on the Creutz Hubbard Hamiltonian to understand better the superfluid behavior. The m-particle excitation energy, i.e., the energy gap per particle to promote such excitation, can be defined as [40,41]

$$\delta_m \equiv \frac{1}{m}[E_0(N+m) + E_0(N-m) - 2E_0(N)], \tag{9}$$

where m is the number of doped particles in a system with N particles; E_0 is the corresponding ground state at those fillings. We first describe the single particle ($m = 1$) excitations in Fig. 7, for the densities $\rho_{\rm f} = 1,\ 1/2$, and $1/4$, as functions of $|U|/t$. They show that the gap to add one particle has small finite size corrections; furthermore, in the regime of strong

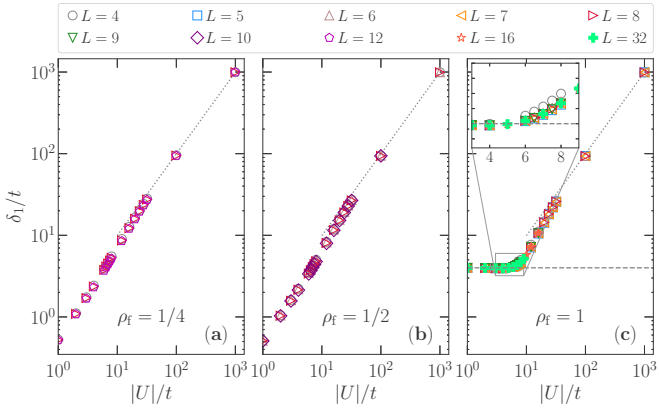

FIG. 7. The one-particle gap energies for $\rho = 1/4$, $1/2$, and 1 as functions of the coupling $|U|/t$. The dotted lines have the form $\delta_1 \propto |U|/t$ and are guides to the eye. For $\rho = 1$ [(c)], the dashed line at $\delta_1 = 4t$ indicates the range of validity of the projected Hamiltonian, where excitations are gapped by the noninteracting Creutz bandwidth. The inset displays in detail the departure from this regime, starting at interactions $|U|/t \gtrsim 4$. As in previous figures, ED (DMRG) results are given by empty (filled) symbols.

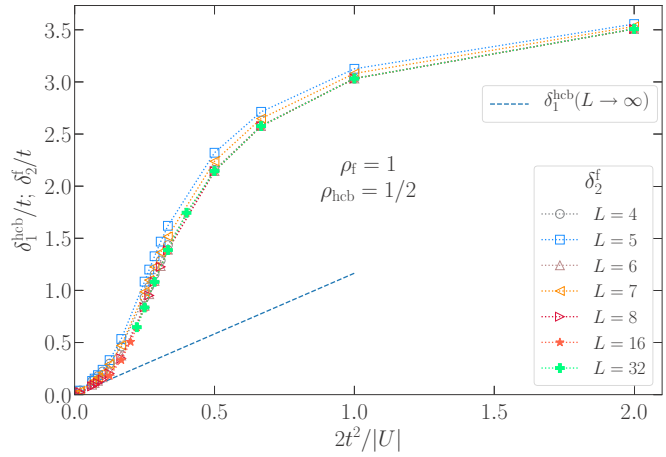

FIG. 9. Single-particle gap for the effective hard core boson model (8), δ_1^{hcb}, and two-particle gap for the original fermionic model (1), δ_2^f, as functions of $2t^2/|U|$. The extrapolation to the thermodynamic limit of δ_1^{hcb} is given by the dashed line, whereas δ_2^f is presented for different system sizes. As in previous figures, ED (DMRG) results are given by empty (filled) symbols.

interactions, the gaps are proportional to $|U|/t$, indicating tighter binding. At small interaction strengths, the behavior of δ_1 is markedly different for different densities. While for $\rho_f < 1$, the single particle gap is finite and proportional to $|U|/t$, at half-filling, $\delta_1 \gtrsim 4t$, suggesting that the single-particle picture, with two flat bands separated by a gap of this same energy, is still applicable. For that density, the lower band is completely filled and the cost in energy to add an extra particle is then $4t$.

Figure 8 shows that the two-particle gaps suffer appreciable finite size effects. Away from half-filling, the dependence of δ_2 on $|U|/t$ suggests that this quantity peaks at interactions corresponding to the maximum of the superfluid weight, $|U|/t \approx 8$. However, finite size scaling analysis [insets in Figs. 8(a) and 8(b)] shows that this pair excitation is gapless,

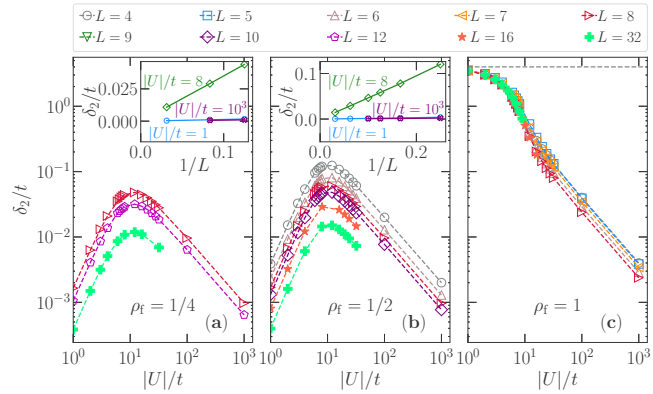

FIG. 8. Similar to Fig. 7, but for two-particle excitations. The dashed line at $\delta_2 = 4t$ in (c) indicates the range of validity of the projected Hamiltonian. As in previous figures, ED (DMRG) results are given by empty (filled) symbol. The insets in (a) and (b) display the finite size scaling of δ_2 for three values of the interactions at densities $\rho_f = 1/4$ and $1/2$, respectively.

as one would expect for a system displaying finite superfluid weight in the thermodynamic limit. For $\rho_f = 1$ and small interactions, the energy per particle to add a pair is again close to the noninteracting gap. It takes values slightly below $4t$ in this regime because the added particles, which populate the upper band, can further decrease their energy by interacting attractively. Most importantly, due to the minimal dependence on system size, one can guarantee that the system is not superfluid, in agreement with the results of Fig. 4 at this filling. In the strongly interacting regime, finite size effects are more pronounced, and δ_2 steadily decreases for larger L's. Nonetheless, we can once again resort to the mapping to the effective Hamiltonian Eq. (8) in this regime, to settle the question whether the two-particle gaps are finite.

In the coupling regime where the pairs are tightly bound, one expects the two-particle fermionic gap [$\delta_2^f \equiv \delta_2$] to correspond to the single-particle gap of hardcore bosons, δ_1^{hcb}, in the effective model language. By performing finite size scaling on the latter, we find that δ_1^{hcb} is finite in the thermodynamic limit as long as the interactions are also finite. Consequently, one expects δ_2^f to be finite too at strong interactions. Figure 9 displays the dependence of δ_2^f and δ_1^{hcb}, at half-filling, as functions of the inverse interaction strength. The agreement of the single particle gap for hardcore bosons and the two-particle gap for fermions is evident at $|U| \gg t$. Essentially, δ_1^{hcb} provides a lower bound to δ_2^f, indicating the gap to create a pair is always finite as long as $|U|$ is. This again confirms the picture that the superfluid weight for $\rho_f = 1$ is zero at arbitrary values of the interactions in the Creutz ladder.

C. Pair correlation functions

The finite gaps for the single-particle excitation suggest that the single-particle Green's function, Eq. (4), should decay exponentially. On the other hand, the high pair mobility indicated by the vanishing of the two-particle excitation energy suggests that the pair Green function, Eq. (3), decays as a

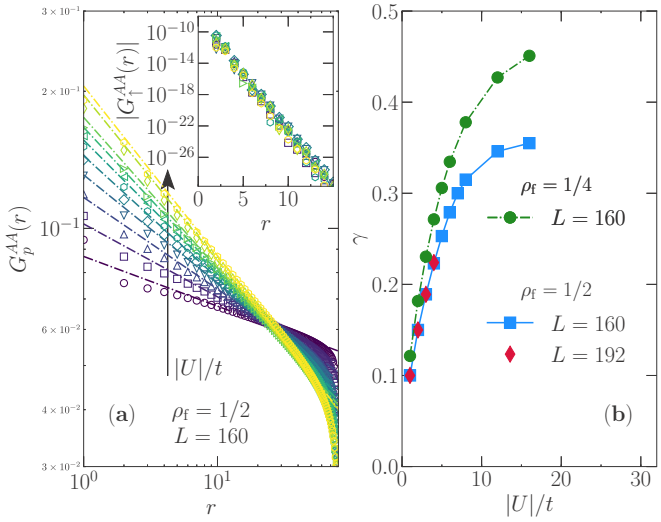

FIG. 10. (a) The intrachain pair correlation function, G_p^{AA} as a function of the distance in a log-log scale and different values of $|U|/t = 1, 2, 3, 4, 5, 6, 7, 8, 12, 16$, as signaled by the vertical arrow. The lattice size is $L = 160$ and $\rho_f = 1/2$. The inset displays the single-particle Green's functions in a linear-logarithm scale. In (b), the dependence on $|U|/t$ of the decay exponent γ of the pair Green function, for densities $\rho_f = 1/4$ and $1/2$. At large attractive interactions, it possesses an asymptotic behavior, saturating at the value corresponding to the decay of single-particle correlations, $\langle b_{j,r}^\dagger b_j \rangle$, of repulsive hardcore bosons in the same geometry and density $\rho_{hcb} = \rho_f/2$. Finite size effects are already rather small for the values of L considered, 160 and 192, at density $\rho_f = 1/2$.

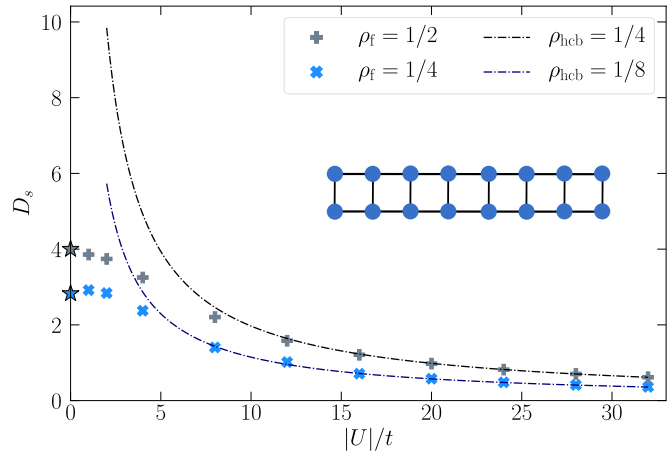

FIG. 11. Drude weight in the thermodynamic limit vs $|U|/t$, for a regular ladder. The noninteracting results, which are finite, unlike in the Creutz lattice, are indicated by the star symbols at $|U|/t = 0$. The strongly interacting regime is explained by the results of repulsive hardcore bosons on a regular ladder, depicted by the dashed-dotted lines.

power with distance, for densities away from half-filling. This is confirmed in the inset of Fig. 10(a), which shows very fast exponential decay of the one-particle Green function with distance, signaling a robust single-particle gap at the density $\rho_f = 1/2$. We have also confirmed that similar behavior occurs for other densities. Moreover, we remark that $\uparrow$ or $\downarrow$ channels, in either chain A or B, result in equivalent values for this correlation.

In contrast, the power-law decay of the pair Green function [Fig. 10(a)] is characteristic of quasi-long range order for this observable, and indicates that local pair excitations are gapless in this system. We note that the larger the attractive interaction the faster is the decay of $G_p^{\alpha\alpha}$ (we use $\alpha = A$). When compiling the values of the decay exponent γ in Fig. 10(b), where $G_p^{\alpha\alpha} \propto r^{-\gamma}$, we note that it essentially saturates at large interactions, denoting that the extent of the decay of the correlations is constant. Once more, we can understand this result via the mapping onto the effective repulsive hardcore boson model in the Creutz geometry Eq. (8). In this case, changing the magnitude of U accounts only for a re-scaling of the Hamiltonian energies, since both hopping and nearest-neighbor interactions have the same energy dependence on $|U|/t$, without changing the decay extent of the correlation functions. Thus one would expect that $\langle \Delta_{j+r}^{\alpha\dagger} \Delta_j^\alpha \rangle \propto \langle b_{j+r}^{\alpha\dagger} b_j^\alpha \rangle \propto r^{-\gamma}$, in the large $|U|/t$ limit.

In (quasi-)one-dimensional systems, repulsive hardcore bosons behave as Luttinger liquids when away from the half-filling regime [42]. We then expect the exponent γ we obtain in the strongly interacting regime to be related to the Luttinger liquid parameter K, which is a function of the density of particles. To the best of our knowledge, this is not known for a system where the interactions and hoppings have the geometry of the Creutz lattice, thus a quantitative prediction is hard to make. Nevertheless, the behavior of D_s, δ_1, δ_2, and the Green functions leads to the conclusion that the attractive Hubbard model in the Creutz lattice, given by Eq. (1), exhibits superfluidity for any $U < 0$, for densities away from half-filling.

D. Regular two-leg ladder

We now compare the above results of the Creutz lattice with the behavior of the attractive fermionic Hubbard model on a simple regular ladder composed of two coupled chains (see Fig. 11). In this case, the Hamiltonian is written as

$$\mathcal{H} = -t \sum_{\langle i,j\rangle,\sigma} (c_{i,\sigma}^\dagger c_{j,\sigma} + \text{H.c.}) + U \sum_j n_{j,\uparrow} n_{j,\downarrow}, \qquad (10)$$

where $\langle i, j \rangle$ indicates inter- and intrachain nearest neighbors and, again, $U < 0$. To start, we highlight the main difference between the Creutz and regular ladders, which is evident when comparing the noninteracting regime. In the Creutz case, as $|U|/t \to 0$, $D_s \to 0$ due to the geometrical localization caused by the flat band; on the other hand, in the ladder case, $|U| \to 0$ leads to a free fermion gas with nonflat dispersion which is mobile.

For finite interactions, we resort to numerical calculations. We calculate the superfluid weight via Eq. (6), by repeating the analysis done for the Creutz lattice. After finite size extrapolations to the thermodynamic limit, we obtain the dependence of D_s on the interaction strength depicted in Fig. 11. As before, one can explain the strongly interacting limit using an effective hardcore boson Hamiltonian similar to Eq. (8), but with hopping and interacting terms corresponding to the ladder geometry. However, in contrast to the Creutz

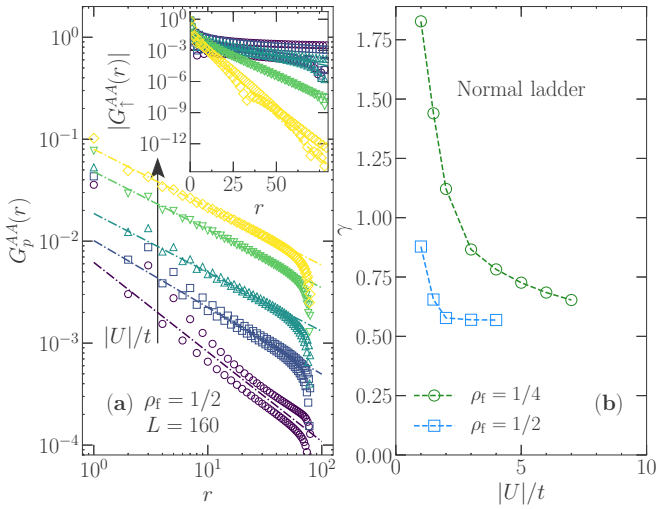

FIG. 12. The same as in Fig. 10, but now in the case of a regular ladder. The interaction values used are $|U|/t = 1,\ 1.5,\ 2,\ 3,$ and 4, and are schematically represented by the vertical arrow.

case, the noninteracting, $U = 0$, result is finite and can be calculated exactly using the energy dispersion of the ladder, $\varepsilon_k = -2t\cos(k) \pm t$. The definition of the superfluid weight [Eq. (6)] yields $D_s(U = 0) = 4t \sin(\pi\rho)$, for $\rho \leqslant 1/2$, i.e., where only the lower band has finite occupancy in the ground state. These are indicated by star symbols in Fig. 11 for the two densities we investigated, $\rho_f = 1/4$ and $1/2$. However, it is very important to keep in mind our discussion after Eq. (6): that $D_s(U = 0)$ is nonzero does not mean that the noninteracting system is superfluid. At $U = 0$, both the single particle and pair Green functions decay as power laws indicating metallic behavior. Our results indicate that (up to the precision of our calculations) as soon as $|U| \neq 0$, the fermions start to pair and form a superfluid phase characterized by exponential decay of the single particle Green function and power law for the pair correlations.

At half-filling, one can apply a particle-hole transformation in one of the spin components, say $\tilde{c}_{i,\downarrow} = (-1)^i c^\dagger_{i,\downarrow}$, keeping the other component unchanged, to map the Hamiltonian onto the repulsive Hubbard model in a two-leg ladder. In this case, one expects a Mott insulating behavior, whose charge stiffness approaches zero in the thermodynamic limit. Hence, in the original Hamiltonian, both the superfluid and Drude weights should also decay to zero when $L \to \infty$, provided the interactions are finite.

Previous studies using zero-temperature quantum Monte Carlo techniques [43] obtained the power-law decay of pair correlations for the normal ladder at $\rho_f = 1/2$. The decay exponent was found to be either $\gamma = 1.07(3)$ or $\gamma = 0.87(2)$, if considering the fitting to the upper or lower envelope of the oscillating pair correlations with distance, for interactions $|U|/t = 2$. Here, we focus on the same density using DMRG. Similarly to Fig. 10, we report in Fig. 12(a) the decay with distance of the pair and single-particle Green's functions. Again, the respective power-law and exponential decays signal the superfluid character of the system and agrees with the predictions of the superfluid weight presented in Fig. 11. Furthermore, we show in Fig. 12(b) the dependence of the decay exponent of the pair Green's functions on the interaction strength. One can highlight two points: the first is that the magnitude of the interactions that yields a saturated exponent is much smaller than in the case of the Creutz lattice (note the different ranges of interactions in both plots). This can be understood by noticing that the agreement of the superfluid weight of hardcore bosons with the one obtained for the original fermionic model (Fig. 11) appears at smaller interactions in comparison to the Creutz lattice (Fig. 5). The second point is that at the same density we have investigated for the Creutz ladder [Fig. 10(b)] the decay exponent is larger for the ladder. This means that the pair correlations, although still displaying algebraic behavior, are shorter ranged for the ladder than for the Creutz lattice at the same density. In that sense, one can argue that the superfluid nature in a Creutz lattice is more robust that in a regular ladder.

IV. CONCLUSIONS AND REMARKS

We investigated the superfluid properties of attractive fermions on a cross-linked ladder using numerical unbiased methods, namely exact diagonalization and density matrix renormalization group. The ladder, known as the Creutz lattice, is constructed in such a away as to render two flat bands in the tight-binding regime. We introduce local attractive interactions between fermions and show that the system displays finite superfluid weight with two distinct regimes, of weak and strong interactions if the fermionic filling is smaller than one. In the former, we show that this quantity is explained by the analysis of a projected Hamiltonian on the lower band, valid at small energy scales [24], whereas in the latter, it can described by the superfluid properties of repulsive hardcore bosons on a similar lattice, but with all the bonds having hopping energies with the same sign.

Quantitative study of single and two-particle excitations of the fermionic problem corroborates this picture, showing that the energy to excite a single charge is gapped for the wide range of interactions we investigate. On the other hand, pairs can be excited without an energy cost for densities $\rho_f < 1$. We further study the single-particle (pair) correlation functions along the ladder, obtaining exponential (power law) decay with distance, denoting gapped (gapless) behavior for this excitation. Finally, we found that power-law decay of pair correlations are slower, often much slower, in the Creutz lattice than in the normal ladder. Note that Fig. 10(b) shows that the decay exponent on the Creutz lattice is always less than $1/2$, while on the ladder, Fig. 12(b) shows it always to be larger than $1/2$ and can even rise above 1. With the Luttinger parameter K, defined as $G(r) \sim 1/r^{(1/2K)}$, this gives $K > 1$ for Creutz and $K < 1$ for the ladder. It is known from bosonization [26] that when $K < 1/2$ (i.e., power decay exponent larger than 1) the superfluid is unstable and can be localized even by a single impurity. In this sense, we say that superfluidity in the Creutz lattice is more robust.

Note added. Upon completion of this manuscript, a preprint appeared which tackled a similar problem [44], also finding formation of pair superfluidity away from half-filling. In addition to obtaining similar results, here we also quantitatively connect the results in the strongly interacting regime to a

repulsive hardcore boson model which is superfluid for any finite interactions. We also show how those are connected to properties of the ground state, as in the single- and pair-correlation functions.

ACKNOWLEDGMENTS

The authors acknowledge insightful discussions with R. Scalettar. R.M. also acknowledges discussions with C. Cheng. R.M. is supported by the National Natural Science Foundation of China (NSFC) Grant Nos. 11674021 and 11650110441; and NSAF-U1530401. GGB is partially supported by the French government, through the UCAJEDI Investments in the reference number ANR-15-IDEX-01. The computations were performed in the Tianhe-2JK at the Beijing Computational Science Research Center (CSRC) and with resources of the National Supercomputing Centre, Singapore (https://www.nscc.sg). This research is supported by the National Research Foundation, Prime Minister's Office, Singapore and the Ministry of Education-Singapore under the Research Centres of Excellence programme.

[1] A. Mielke, Exact ground states for the Hubbard model on the Kagome lattice, J. Phys. A: Math. Gen. **25**, 4335 (1992).
[2] H. Aoki, M. Ando, and H. Matsumura, Hofstadter butterflies for flat bands, Phys. Rev. B **54**, R17296 (1996).
[3] S. Deng, A. Simon, and J. Köhler, The origin of a flat band, J. Solid State Chem. **176**, 412 (2003), special issue on The Impact of Theoretical Methods on Solid-State Chemistry.
[4] C. Wu, D. Bergman, L. Balents, and S. Das Sarma, Flat Bands and Wigner Crystallization in the Honeycomb Optical Lattice, Phys. Rev. Lett. **99**, 070401 (2007).
[5] H. Tasaki, Hubbard model and the origin of ferromagnetism, Eur. Phys. J. B **64**, 365 (2008).
[6] Z. Lan, N. Goldman, and P. Öhberg, Coexistence of spin-$\frac{1}{2}$ and spin-1 Dirac-Weyl fermions in the edge-centered honeycomb lattice, Phys. Rev. B **85**, 155451 (2012).
[7] T. Jacqmin, I. Carusotto, I. Sagnes, M. Abbarchi, D. D. Solnyshkov, G. Malpuech, E. Galopin, A. Lemaître, J. Bloch, and A. Amo, Direct Observation of Dirac Cones and a Flatband in a Honeycomb Lattice for Polaritons, Phys. Rev. Lett. **112**, 116402 (2014).
[8] E. H. Lieb, Two Theorems on the Hubbard Model, Phys. Rev. Lett. **62**, 1201 (1989).
[9] B. Sutherland, Localization of electronic wave functions due to local topology, Phys. Rev. B **34**, 5208 (1986).
[10] V. I. Iglovikov, F. Hébert, B. Grémaud, G. G. Batrouni, and R. T. Scalettar, Superconducting transitions in flat-band systems, Phys. Rev. B **90**, 094506 (2014).
[11] T. T. Heikkilä and G. E. Volovik, Flat bands as a route to high-temperature superconductivity in graphite, in *Basic Physics of Functionalized Graphite*, edited by P. D. Esquinazi (Springer International Publishing, Cham, 2016), pp. 123–143.
[12] Y. Cao, V. Fatemi, S. Fang, K. Watanabe, T. Taniguchi, E. Kaxiras, and P. J-Herrero, Unconventional superconductivity in magic-angle graphene superlattices, Nature (London) **556**, 43 (2018).
[13] S. D. Huber and E. Altman, Bose condensation in flat bands, Phys. Rev. B **82**, 184502 (2010).
[14] M. Creutz, End States, Ladder Compounds, and Domain-Wall Fermions, Phys. Rev. Lett. **83**, 2636 (1999).
[15] T. Misumi and H. Aoki, New class of flat-band models on tetragonal and hexagonal lattices: Gapped versus crossing flat bands, Phys. Rev. B **96**, 155137 (2017).
[16] B. Douçot and J. Vidal, Pairing of Cooper Pairs in a Fully Frustrated Josephson-Junction Chain, Phys. Rev. Lett. **88**, 227005 (2002).
[17] M. Rizzi, V. Cataudella, and R. Fazio, 4*e*-condensation in a fully frustrated Josephson junction diamond chain, Phys. Rev. B **73**, 100502 (2006).
[18] A. A. Lopes and R. G. Dias, Interacting spinless fermions in a diamond chain, Phys. Rev. B **84**, 085124 (2011).
[19] B. Grémaud and G. G. Batrouni, Haldane phase on the sawtooth lattice: Edge states, entanglement spectrum, and the flat band, Phys. Rev. B **95**, 165131 (2017).
[20] S. Takayoshi, H. Katsura, N. Watanabe, and H. Aoki, Phase diagram and pair Tomonaga-Luttinger liquid in a Bose-Hubbard model with flat bands, Phys. Rev. A **88**, 063613 (2013).
[21] M. Tovmasyan, E. P. L. van Nieuwenburg, and S. D. Huber, Geometry-induced pair condensation, Phys. Rev. B **88**, 220510 (2013).
[22] D. Sticlet, L. Seabra, F. Pollmann, and J. Cayssol, From fractionally charged solitons to majorana bound states in a one-dimensional interacting model, Phys. Rev. B **89**, 115430 (2014).
[23] S. Peotta and Päivi Törmä, Superfluidity in topologically nontrivial flat bands, Nat. Commun. **6**, 8944 (2015), article.
[24] M. Tovmasyan, S. Peotta, Päivi Törmä, and S. D. Huber, Effective theory and emergent SU(2) symmetry in the flat bands of attractive Hubbard models, Phys. Rev. B **94**, 245149 (2016).
[25] S. Ryu, A. P. Schnyder, A. Furusaki, and A. W. W. Ludwig, Topological insulators and superconductors: tenfold way and dimensional hierarchy, New J. Phys. **12**, 065010 (2010).
[26] T. Giamarchi, *Quantum Physics in One Dimension* (Oxford University Press, Oxford, 2004).
[27] E. Fradkin, *Quantum Physics in One Dimension*, 2nd ed. (Cambridge University Press, Cambridge, UK, 2013).
[28] S. R. White, Density Matrix Formulation for Quantum Renormalization Groups, Phys. Rev. Lett. **69**, 2863 (1992).
[29] S. R. White, Density-matrix algorithms for quantum renormalization groups, Phys. Rev. B **48**, 10345 (1993).
[30] W. Kohn, Theory of the insulating state, Phys. Rev. **133**, A171 (1964).
[31] X. Zotos, P. Prelovek, and I. Sega, Single-hole effective masses in the t-J model, Phys. Rev. B **42**, 8445 (1990).
[32] B. S. Shastry and B. Sutherland, Twisted Boundary Conditions and Effective Mass in Heisenberg-Ising and Hubbard Rings, Phys. Rev. Lett. **65**, 243 (1990).
[33] R. M. Fye, M. J. Martins, D. J. Scalapino, J. Wagner, and W. Hanke, Drude weight, optical conductivity, and flux properties of one-dimensional Hubbard rings, Phys. Rev. B **44**, 6909 (1991).

[34] D. J. Scalapino, S. R. White, and S. Zhang, Insulator, metal, or superconductor: The criteria, Phys. Rev. B **47**, 7995 (1993).

[35] C. A. Hayward, D. Poilblanc, R. M. Noack, D. J. Scalapino, and W. Hanke, Evidence for a Superfluid Density in t-J Ladders, Phys. Rev. Lett. **75**, 926 (1995).

[36] V. G. Rousseau, The superfluid density in continuous and discrete spaces: Avoiding misconceptions, Phys. Rev. B **90**, 134503 (2014).

[37] R. Micnas, J. Ranninger, and S. Robaszkiewicz, Superconductivity in narrow-band systems with local nonretarded attractive interactions, Rev. Mod. Phys. **62**, 113 (1990).

[38] N. Byers and C. N. Yang, Theoretical Considerations Concerning Quantized Magnetic Flux in Superconducting Cylinders, Phys. Rev. Lett. **7**, 46 (1961).

[39] C. N. Yang, Concept of off-diagonal long-range order and the quantum phases of liquid He and of superconductors, Rev. Mod. Phys. **34**, 694 (1962).

[40] J. F. Dodaro, H.-C. Jiang, and S. A. Kivelson, Intertwined order in a frustrated four-leg t-J cylinder, Phys. Rev. B **95**, 155116 (2017).

[41] J. Jünemann, A. Piga, S.-J. Ran, M. Lewenstein, M. Rizzi, and A. Bermudez, Exploring Interacting Topological Insulators with Ultracold Atoms: The Synthetic Creutz-Hubbard Model, Phys. Rev. X **7**, 031057 (2017).

[42] F. Crépin, N. Laflorencie, G. Roux, and P. Simon, Phase diagram of hard-core bosons on clean and disordered two-leg ladders: Mott insulator–Luttinger liquid–Bose glass, Phys. Rev. B **84**, 054517 (2011).

[43] M. Guerrero, G. Ortiz, and J. E. Gubernatis, Pairing correlations in the attractive Hubbard model on chains, ladders, and squares, Phys. Rev. B **62**, 600 (2000).

[44] M. Tovmasyan, S. Peotta, L. Liang, P. Törmä, and S. D. Huber, Preformed pairs in flat Bloch bands, Phys. Rev. B **98**, 134513 (2018).